J Geod (2006) 79: 586–601
DOI 10.1007/s00190-005-0008-6

ORIGINAL ARTICLE

P. Ditmar · V. Kuznetsov · A. A. van Eck van der Sluijs
E. Schrama · R. Klees

'DEOS_CHAMP-01C_70': a model of the Earth's gravity field computed from accelerations of the CHAMP satellite

Received: 13 September 2004 / Accepted: 29 September 2005 / Published online: 3 December 2005

Abstract Performance of a recently proposed technique for gravity field modeling has been assessed with data from the CHAMP satellite. The modeling technique is a variant of the acceleration approach. It makes use of the satellite accelerations that are derived from the kinematic orbit with the 3-point numerical differentiation scheme. A 322-day data set with 30-s sampling has been used. Based on this, a new gravity field model – DEOS_CHAMP-01C_70 - is derived. The model is complete up to degree and order 70. The geoid height difference between the DEOS_CHAMP-01C_70 and EIGEN-GRACE01S models is 14 cm. This is less than for two other recently published models: EIGEN-CHAMP03Sp and ITG-CHAMP01E. Furthermore, we analyze the sensitivity of the model to some empirically determined parameters (regularization parameter and the parameter that controls the frequency-dependent data weighting). We also show that inaccuracies related to non-gravitational accelerations, which are measured by the on-board accelerometer, have a minor influence on the computed gravity field model.

Keywords Earth's gravity field · Satellite accelerations · Acceleration approach · CHAMP · DEOS_CHAMP-01C_70

1 Introduction

Challenging minisatellite payload (CHAMP) is a German satellite mission launched in 2000 for geoscientific and atmospheric research and applications (Reigber et al. 1996). To facilitate studies of the Earth's gravity field, the satellite is equipped with a high-quality GPS receiver as well as with a 3-axis accelerometer to measure non-gravitational forces that influence the satellite motion (e.g. the atmospheric drag).

P. Ditmar (✉)· V. Kuznetsov · A.A. van Eck van der Sluijs
E. Schrama · R. Klees
Delft Institute of Earth Observation and Space Systems (DEOS)
Faculty of Aerospace Engineering, Delft University of Technology,
Kluyverweg 1, 2629 HS, Delft, The Netherlands
E-mail: p.ditmar@lr.tudelft.nl
Tel.: +31-15-2782501
Fax: +31-15-2783711

Computation of gravity field parameters from a satellite orbit has been a research issue for a number of decades (see e.g., O'Keefe, 1957; Ilk 1984; Schrama 1986; Reigber 1989). However, the launch of the CHAMP mission has triggered a rebirth of interest in this subject. A number of models have been obtained from CHAMP data with the approach based on integration of the variational equations, when the functional model makes use of GPS data or of the satellite orbit (Reigber et al. 2002, 2003a,b,c, 2005a). An alternative approach has been used by Ilk et al. (2003, 2005) and Mayer-Gürr et al. (2005), who exploted a linear functional model connecting the satellite orbit with gravity field parameters (Ilk, 1984). There have been also attempts to derive a gravity field model using the energy balance approach, which is based on the measured kinetic energy of the satellite (Sneeuw et al. 2002; Han et al. 2002; Howe et al. 2003; Gerlach et al. 2003a,b). Besides, the acceleration approach has been tried, when the observed satellite accelerations are exploited (Reubelt et al. (2003a,b); Fengler et al. (2004)). In this paper, we follow a new technique (Ditmar and van Eck van der Sluijs 2004), which is a variant of the acceleration approach. Our objectives are to assess the performance of the proposed technique with data from the CHAMP mission and to compare the computed Earth's gravity field model with those obtained from CHAMP data in alternative ways.

The technique under consideration is based on satellite accelerations that are derived from an orbit with the three-point difference scheme:

$$\bar{\mathbf{a}}(t) = \frac{\mathbf{x}(t-\Delta t) - 2\mathbf{x}(t) + \mathbf{x}(t+\Delta t)}{(\Delta t)^2}, \qquad (1)$$

where $\mathbf{x}(t)$ is the satellite position vector at time t, Δt is the data sampling interval, and $\bar{\mathbf{a}}(t)$ is the derived acceleration. The motivation to use only three orbit points for deriving accelerations is the following: (1) less information is lost in the presence of data gaps (in comparison with a multi-point differentiation scheme) and (2) the covariance matrix of acceleration noise can be easier determined and inverted. It is important that the accelerations are derived in an inertial

frame. Ditmar and van Eck van der Sluijs (2004) have shown that the accelerations $\bar{\mathbf{a}}(t)$ in Eq. (1) are weighted averages:

$$\bar{\mathbf{a}}(t) = \int_{-\Delta t}^{\Delta t} w(s)\,\mathbf{a}(t+s)\,ds, \tag{2}$$

where the weight function $w(s)$ is a piece-wise linear function:

$$w(s) = \frac{\Delta t - |s|}{(\Delta t)^2}. \tag{3}$$

It is interesting to note that our approach can be linked to the one of Ilk et al. (2003), provided that the arc length in the latter approach is set equal to the double sampling interval.

We would like to stress that it is advisable to derive accelerations from a kinematic orbit, i.e., the orbit determined directly from GPS measurements without any information about forces that influence the satellite motion. Though a kinematic orbit may contain numerous interruptions and relatively large noise at high frequencies, it is, unlike a reduced-dynamic orbit, not directly influenced by any existing gravity field model. Therefore, we fully control the stochastic properties of input data and can build the optimal procedure for their processing. As far as noise is concerned, it can be suppressed later in well-known ways (e.g., by means of a regularization technique).

The accelerations derived from the satellite orbit are an input to produce residual acceleration, i.e., those that cannot be explained by models. In doing so, we deduce the reference accelerations, which are computed on the basis of a reference gravity field model and tide models. Furthermore, non-gravitational accelerations, which are measured by the accelerometer on board the satellite, are deduced as well. The residual accelerations are used to compute spherical harmonic coefficient corrections. The computed corrections are summed with the spherical harmonic coefficients from the reference model, yielding the final product: a new model of the static gravity field of the Earth. A general flow-chart of the data processing is shown in Fig. 1.

Section 2 contains a detailed description of how we derived residual satellite acceleration from the CHAMP orbit. Furthermore, this section explains how the gravity field model is obtained from these accelerations. Section 3 is devoted to the analysis of the model obtained and to its comparison with some other models based on CHAMP data.

2 Data processing

2.1 Input data

In our computations, we have used a set of CHAMP data from March 10, 2002 to January 25, 2003 (in total, 322 days). The data set contains six 1-day gaps and two-day gaps. Apart from the primary data set – the kinematic orbit — some additional data were also used: accuracy description of the kinematic orbit in the form of a 3×3 position covariance matrix per epoch and a reduced-dynamic satellite orbit. The latter one is a result of an orbit integration based on given force model; once per 6 min, the orbit experiences a discontinuity in terms of velocities so that a consistency with on-board GPS measurements is preserved. All these data were kindly provided to us by D. Švehla and M. Rothacher, Technical University Munich (Švehla and Rothacher 2003). The data were defined relatively to the ITRF2000 datum (IGS00 realization). Besides, we have used the CHAMP accelerometer and star camera data distributed by CHAMP's Information System and Data Center (ISDC) at GeoForschungsZentrum Potsdam (GFZ).

2.2 Inertial frame

An inertial frame is used not only for derivation of accelerations from the satellite orbit but also in some other procedures that will be addressed later. The inertial frame we use is the Celestial Reference Frame (CRF); all the transformations from the Terrestrial Reference Frame (TRF) to the CRF and back are performed in compliance with the IERS conventions 2003 (McCarthy and Petit 2003).

2.3 Local orbital reference frame

Prior to gravity field modeling, a rotation operation is applied in order to transform the accelerations from the CRF into the Local Orbital Reference Frame (LORF). The axes of the LORF are defined as follows: the X-axis is directed along the track, the Y-axis coincides with the direction of the orbital angular momentum and the Z-axis completes the frame to a right-handed one. There are at least two reasons to use the LORF in the definition of the functional model: (1) the consistency with non-gravitational acceleration measurements (the orientation of the on-board accelerometer axes is very close to the LORF) and (2) a dominant block-diagonal structure of the normal matrix in that case, which leads to a numerically efficient data processing scheme. The latter aspect has been already considered in detail by Ditmar and van Eck van der Sluijs (2004).

In order to transform an arbitrary three-component vector from the TRF into the LORF, the rotation matrix $\mathbf{R}_{\mathbf{TRF}\to\mathbf{LORF}}$ has to be applied. This matrix represents a composition of four elementary rotations:

$$\mathbf{R}_{\mathbf{TRF}\to\mathbf{LORF}} = \mathbf{R}_{\mathbf{y}}(-\alpha)\,\mathbf{R}_{\mathbf{z}}(-\beta)\,\mathbf{R}_{\mathbf{y}}(-\theta)\,\mathbf{R}_{\mathbf{z}}(\lambda-\pi), \tag{4}$$

where λ is the longitude of the current point, θ is its (geocentric) co-latitude, α is the angle between the horizon and the satellite velocity vector, and β is the azimuth of the satellite velocity vector, i.e., is the (clockwise) angle between the northward direction and the projection of the velocity vector onto the horizontal plane. The velocity should be defined relatively to the CRF.

In order to determine the satellite velocity at a particular point, we use the reduced-dynamic orbit because it represents the satellite motion more accurately than the kinematic orbit. The velocity is derived with a 13-point numerical differentiation scheme (the scheme is defined on the basis of the

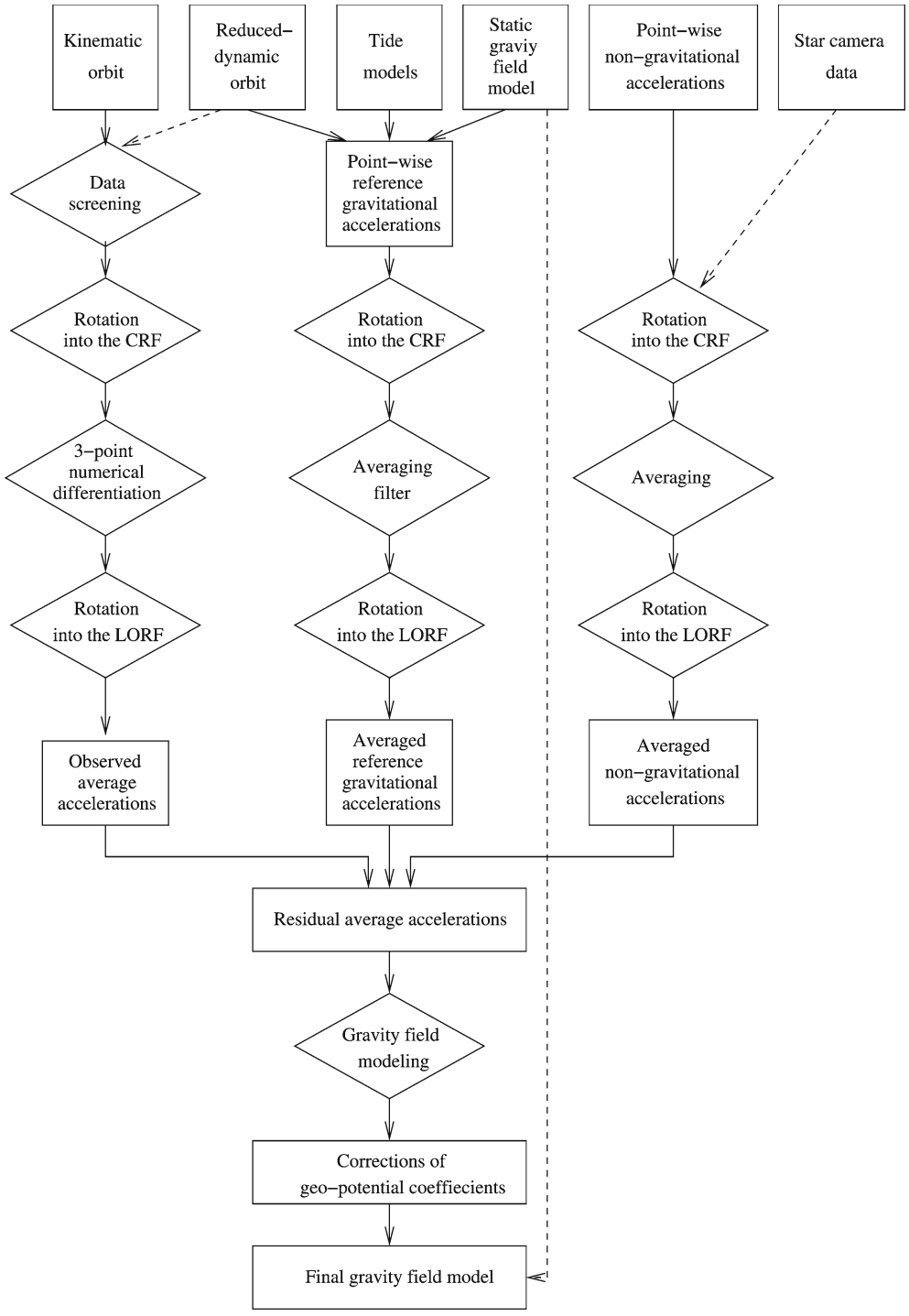

Fig. 1 Flow-chart of data processing

Taylor expansion of the function to be differentiated around the central point)

2.4 Derivation of the observed satellite accelerations

The stochastic description of the kinematic orbit, which is provided in the form of a 3×3 position covariance matrix per epoch $\mathbf{Q}_j^{(\mathbf{TRF})}$, plays an important role in the data processing. To stay consistent with the definition of the functional model, we rotate these covariance matrices into the LORF:

$$\mathbf{Q}_j^{(\mathbf{LORF})} = \mathbf{R}_{\mathbf{TRF}\rightarrow\mathbf{LORF}}\, \mathbf{Q}_j^{(\mathbf{TRF})}\, \mathbf{R}_{\mathbf{LORF}\rightarrow\mathbf{TRF}}. \quad (5)$$

Then we determine the positioning errors in the LORF for a given epoch by taking the square root of the diagonal

Table 1 Statistics of position data screening

Category	Number of epochs	Percentage of the total number
Absent kinematic position or covariance matrix	94,290	10.2
Position error > 5 cm	22,959	2.5
Distance between the kinematic and reduced-dynamic orbit > 50 cm	13,216	1.4
Identified as outliers	38,875	4.2
Passed all the tests	758,020	81.7
Total for 322 days	927,360	100.0

elements of the matrix $\mathbf{Q}_{\mathbf{j}}^{(\mathbf{LORF})}$. These errors are used for a preliminary data screening. If at least one of the components of the positioning error exceeds a given threshold (5 cm), the epoch is discarded. Furthermore, there are epochs not supplied with covariance matrices at all; such epochs are also discarded.

The next data processing stage is to compute the orbit discrepancies $\Delta\mathbf{y}_{\mathbf{j}}^{(\mathbf{TRF})}$ as differences between the kinematic and the reduced-dynamic orbits:

$$\Delta\mathbf{y}_{\mathbf{j}}^{(\mathbf{TRF})} = \mathbf{y}_{\mathbf{j}}^{(\mathbf{kin})} - \mathbf{y}_{\mathbf{j}}^{(\mathbf{rd})}. \tag{6}$$

The orbit discrepancies are also rotated into the LORF:

$$\Delta\mathbf{y}_{\mathbf{j}}^{(\mathbf{LORF})} = \mathbf{R}_{\mathbf{TRF}\rightarrow\mathbf{LORF}}\,\Delta\mathbf{y}_{\mathbf{j}}^{(\mathbf{TRF})}. \tag{7}$$

The rotated orbit discrepancies are used in the further data screening. First of all, we eliminate the epochs when the length of the discrepancy vector exceeds a given threshold (50 cm). After that, we run a procedure for the identification of orbit discontinuities. These discontinuities frequently correspond to epochs when the number of visible GPS satellites changes. The orbit discontinuities do not reflect the physical motion of the satellite. It is, therefore, important to exclude the epochs when a discontinuity is observed, otherwise the gravity field model can be distorted.

The identification procedure uses the time-differences of the orbit discrepancies $\Delta\mathbf{y}_{\mathbf{j,j+1}} \equiv \Delta\mathbf{y}_{\mathbf{j+1}}^{(\mathbf{LORF})} - \Delta\mathbf{y}_{\mathbf{j}}^{(\mathbf{LORF})}$ (the superscript "LORF" is omitted for brevity). Our basic assumption is that these differences reflect, generally speaking, random noise in the kinematic orbit. The influence of other factors, like noise in the reduced-dynamic orbit and a signal in the kinematic orbit not explained by the reduced-dynamic orbit, is neglected. Furthermore, noise in kinematically determined positions is assumed to be Gaussian, non-correlated in time and having zero mean. Under these assumptions, the vector $\Delta\mathbf{y}_{\mathbf{j,j+1}}$ is a random vector with zero mean and the covariance matrix $\mathbf{Q}_{\mathbf{j,j+1}}$:

$$\mathbf{Q}_{\mathbf{j,j+1}} = \mathbf{U}\tilde{\mathbf{Q}}_{\mathbf{j,j+1}}\mathbf{U}^{\mathrm{T}}, \tag{8}$$

where matrix $\mathbf{U}$ is defined as:

$$\mathbf{U} = \begin{pmatrix} -1 & 0 & 0 & 1 & 0 & 0 \\ 0 & -1 & 0 & 0 & 1 & 0 \\ 0 & 0 & -1 & 0 & 0 & 1 \end{pmatrix}, \tag{9}$$

and $\tilde{\mathbf{Q}}_{\mathbf{j,j+1}}$ is the 6×6 matrix:

$$\tilde{\mathbf{Q}}_{\mathbf{j,j+1}} = \begin{pmatrix} \mathbf{Q}_{\mathbf{j}}^{(\mathbf{LORF})} & 0 \\ 0 & \mathbf{Q}_{\mathbf{j+1}}^{(\mathbf{LORF})} \end{pmatrix}. \tag{10}$$

An orbit discontinuity manifests itself as an outlier in the series of $\Delta\mathbf{y}_{\mathbf{j,j+1}}$. To detect such an outlier, we execute the generalized likelihood ratio test (Teunissen 2000). Two hypotheses about the expectation of the vector $\Delta\mathbf{y}_{\mathbf{j,j+1}}$ are considered:

$$H_0 : E\{\Delta\mathbf{y}_{\mathbf{j,j+1}}\} = \mathbf{0} \quad \text{versus} \quad H_{\mathrm{A}} : E\{\Delta\mathbf{y}_{\mathbf{j,j+1}}\} \neq \mathbf{0}. \tag{11}$$

Acceptance of the hypothesis H_{A} means that the current vector $\Delta\mathbf{y}_{\mathbf{j,j+1}}$ is identified as an outlier. In order to make the decision, we compute

$$\eta = \Delta\mathbf{y}_{\mathbf{j,j+1}}^{\mathrm{T}}\mathbf{Q}_{\mathbf{j,j+1}}^{-1}\Delta\mathbf{y}_{\mathbf{j,j+1}}. \tag{12}$$

From the definition of $\mathbf{Q}_{\mathbf{j,j+1}}$ and $\Delta\mathbf{y}_{\mathbf{j,j+1}}$, it follows that η must be a random value characterized by the distribution $\chi^2(3, 0)$. We compare η with a certain threshold $k(\alpha)$, which is a function of the probability in the right-hand tail α_p. The hypothesis H_{A} is accepted if $\eta > k(\alpha_p)$: in this case the deviation of the vector $\Delta\mathbf{y}_{\mathbf{j,j+1}}$ from zero is too large to be explained by random noise in the kinematic orbit. Identification of the vector $\Delta\mathbf{y}_{\mathbf{j,j+1}}$ as an outlier leads to the exclusion of both epochs j and $j + 1$ from the further data processing. After several tries, the threshold $k(\alpha_p)$ was set equal to 2.366, which corresponds to $\alpha_p = 0.50$.

Some statistical information regarding CHAMP data screening is shown in Table 1. Surprisingly, the outlier detection procedure has discarded less than 5% of the data (the specified threshold suggests that as much as 50% of differences $\Delta\mathbf{y}_{\mathbf{j,j+1}}$ are to be identified as outliers for purely statistical reasons). Such a discrepancy can be probably explained by an imperfectness of the available statistical information about noise in the kinematic orbit (overestimated noise magnitude or/and neglected temporal correlations).

The kinematically determined positions that passed all the tests (cf. Table 1) were used to derive the accelerations of the CHAMP satellite. These position vectors were transformed from the TRF into the CRF, after which the numerical differentiation of Eq. (1) was applied. Finally, the accelerations were transformed into the LORF. In this way, 717,776 three-component acceleration vectors were produced (77.4% of the total number of epochs in the 322-day time interval).

2.5 Computation of the reference accelerations

Computation of the reference accelerations is performed in two steps: (1) computation of point-wise reference accelerations and (2) averaging. The point-wise reference accelerations are computed on the basis of the EGM96 model of

Table 2 Statistics of accelerometer and star camera data screening

Category	Number of data	Percentage of the total number
Totally absent observations	14,795	0.5
Absent star camera observations	118,563	4.3
Complete observations	2,648,722	95.2
Total for 322 days	2,782,080	100.0

the Earth's static gravity field (Lemoine et al. 1998). Furthermore, astronomic (direct), solid Earth, and ocean tides are taken into account. Astronomic and solid Earth tides are modeled both for the Sun and the Moon, using the DE405 ephemerides (Standish 1998); the influence of planets is neglected. The tidal potential is represented by a spherical harmonic expansion complete to degree 4 (Lambeck 1988; Schrama 1995). In computations of the solid Earth tides, the Earth is assumed to be elastic and spherically symmetric; Love numbers are specified in compliance with the PREM model (Dziewonski and Anderson 1981): $k_2 = 0.303$, $k_3 = 0.0937$, $k_4 = 0.0423$. The ocean tides are modeled according to the GOT00.2 model [which is an update of an earlier model GOT99.2, (Ray 1999)] with eight largest diurnal and semi-diurnal constituents taken into account: Q1, O1, P1, K1, N2, M2, S2, and K2. For each constituent, the corresponding potential is transformed into a spherical harmonic expansion up to degree and order 24. The load Love numbers are defined in compliance with the IERS conventions: $k_2' = -0.3075$, $k_3' = -0.195$, $k_4' = -0.132$, $k_5' = -0.1032$, and $k_6' = -0.0892$ (McCarthy and Petit 2004).

To be consistent with our functional model, the point-wise accelerations have to be transformed into averaged ones. According to Eq. (2), the most straightforward way to do so is just a numerical integration. This would require, however, a sufficiently dense distribution of points at which the point-wise accelerations are known (much denser than the data sampling interval). To make the computations faster, we have used instead an alternative algorithm proposed by Ditmar and van Eck van der Sluijs (2004), which does not require the reference accelerations to be computed with a smaller sampling rate than that of the observed average accelerations. In brief, the algorithm is as follows. A set of point-wise accelerations is computed at the points of the reduced-dynamic orbit with the same sampling interval as that of the observed accelerations: 30 s (at this stage, the reduced-dynamic orbit is superior to the kinematic orbit because the latter one suffers from high-frequency noise). As long as a satellite orbit is a very smooth curve, it is fair to assume that a set of point-wise accelerations to be integrated in compliance with Eq. (2) can be accurately approximated by a high-order polynomial (in practice, a 16-order polynomial is used). Then, the integral of Eq. (2) can be computed analytically. Besides, it can be shown that the value of this integral depends on the point-wise accelerations linearly, and the proportionality coefficients are independent of time (Ditmar and van Eck van der Sluijs 2004). Therefore, transformation of point-wise accelerations into averaged ones can be realized by applying a proper filter, which is called hereafter "averaging filter". It is important that this operation is performed in the CRF. The computed averaged accelerations have to be rotated into the LORF.

2.6 Processing of non-gravitational satellite accelerations

Information about non-gravitational accelerations is provided by the accelerometer on board the CHAMP satellite. This information is given in the accelerometer instrument reference frame which can be related to the CRF, thanks to the star camera data. In the distributed files, both types of data are given as point-wise values with a 10-s sampling. There is a limited amount of epochs when the sensor measurements are incomplete: either both types of data or only star camera data are absent. In both cases, such epochs are excluded from the further consideration. Some statistical information regarding the satellite sensor data is given in Table 2.

The set of complete sensor measurements has been used in the further processing. First of all, we have transformed non-gravitational accelerations into the CRF. The next task was to convert these measurements into averaged accelerations with the 30-s sampling. As follows from Eqs. (2) and (3), the average acceleration at time t is equal to:

$$\bar{\mathbf{a}}(t) = \frac{1}{900} \int_{-30}^{30} (30 - |s|)\, \mathbf{a}(t+s)\, \mathrm{ds}. \tag{13}$$

The values of the function $\mathbf{a}(t+s)$ at epochs $t-30$, $t-20$, $\ldots$, $t+30$ are just measured non-gravitational accelerations, i.e., are known. Hence Eq. (13) can be approximated by a numerical integration formula. As long as a series of non-gravitational accelerations can be well approximated by a smooth function, a simple trapezium rule can be used, which yields:

$$\bar{\mathbf{a}}(t) = \frac{1}{9} \left(\mathbf{a}(t-20) + 2\mathbf{a}(t-10) + 3\mathbf{a}(t) + 2\mathbf{a}(t+10) + \mathbf{a}(t+20)\right). \tag{14}$$

If sensor data are absent at one or more of five epochs in Eq. (14), the output value is not computed, and the current epoch t is excluded from the further data processing. In this way, we have produced a series of 834,437 three-component data with 30-s sampling. The final stage of accelerometer data processing is the transformation of the averaged non-gravitational accelerations into the LORF.

2.7 Residual accelerations and observation equations

Elements of the data vector **d** that consists of residual satellite accelerations are computed as follows:

$$d_j = a_j^{(\mathrm{obs})} - a_j^{(\mathrm{ref})} - a_j^{(\mathrm{ng})}, \tag{15}$$

where $a_j^{(\mathrm{obs})}$ are the observed accelerations derived as discussed in Sect. 2.4, $a_j^{(\mathrm{ref})}$ are the reference accelerations computed as explained in Sect. 2.5, $a_j^{(\mathrm{ng})}$ are the non-gravitational accelerations obtained as discussed in Sect. 2.6, and the index j indicates a given component at a given epoch. We would like to remind that all these quantities should be understood as average ones and rotated into the LORF.

An element of the data vector is produced only when all three input quantities - $a_j^{(\mathrm{obs})}$, $a_j^{(\mathrm{ref})}$, and $a_j^{(\mathrm{ng})}$ - are available. In this way, we have produced a data vector consisting of 3×666,581 elements. From these data, the Earth's gravity field model or, more specifically, a set of corrections to the reference spherical harmonic coefficients, is computed. In doing so, we take into account an imperfectness of the satellite accelerometer: its readings may suffer from inaccurately determined scale factors and, furthermore, can be biased. For simplicity, we do not distinguish the imperfectness of original accelerometer readings as distributed by the GeoForschungsZentrum (i.e., point-wise non-gravitational accelerations in the accelerometer instrument reference system) and the preprocessed non-gravitational accelerations $a_j^{(\mathrm{ng})}$. Our motivation is as follows: (1) the satellite attitude control system maintains the satellite attitude to be very close to the LORF; and (2) the difference between point-wise and averaged non-gravitational accelerations is minor because they vary slowly in time. For each data component, the scale factor correction and the bias is estimated once per a 10-day interval.

To begin with, consider the problem of an unknown scale factor in non-gravitational accelerations. Let us write the observation equations as follows:

$$\sum_i A_{ji}^{(\mathrm{gr})} x_i^{(\mathrm{gr})} + \left(1 + c_{k(j)}\right) a_j^{(\mathrm{ng})} = a_j^{(\mathrm{obs})} - a_j^{(\mathrm{ref})}, \tag{16}$$

where $x_i^{(\mathrm{gr})}$ are unknown spherical harmonic coefficient corrections, $A_{ji}^{(\mathrm{gr})}$ are design matrix elements related to the gravity field parameters, and $c_{k(j)}$ are residual accelerometer scale factors (i.e., the scale factor corrections) each of which is related to the corresponding time interval $k(j)$. Subtraction of the measured non-gravitational acceleration $a_j^{(\mathrm{ng})}$ from both parts of Eq. (16) yields:

$$\sum_i A_{ji}^{(\mathrm{gr})} x_i^{(\mathrm{gr})} + c_{k(j)} a_j^{(\mathrm{ng})} = d_j. \tag{17}$$

Thus, the problem of unknown accelerometer scale factors can be solved by just adding the corresponding corrections $c_{k(j)}$ to the list of unknown parameters. The price to pay is an increased number of unknown parameters, which makes the data processing somewhat more time-consuming.

Now let us consider the problem of bias. In principle, a bias can be handled similarly to an unknown scale factor: by extending the list of unknown parameters further. We find it, however, more elegant to use another approach. Let the observation equations of Eq. (17) be represented in the matrix form as follows:

$$\mathbf{Ax} = \mathbf{d}, \tag{18}$$

where **x** is the vector of all unknown parameters and **A** is the complete design matrix:

$$\mathbf{x} = \begin{pmatrix} x_1^{(\mathrm{gr})} \\ \vdots \\ x_M^{(\mathrm{gr})} \\ c_{k(1)} \\ \vdots \\ c_{k(N)} \end{pmatrix};$$

$$\mathbf{A} = \begin{pmatrix} A_{11}^{(\mathrm{gr})} & \dots & A_{1M}^{(\mathrm{gr})} & a_1^{(\mathrm{ng})} & 0 & \dots & \dots & 0 \\ A_{21}^{(\mathrm{gr})} & \dots & A_{2M}^{(\mathrm{gr})} & a_2^{(\mathrm{ng})} & 0 & \dots & \dots & 0 \\ \vdots & & \vdots & & \dots & \dots & \dots & \dots \\ A_{N1}^{(\mathrm{gr})} & \dots & A_{NM}^{(\mathrm{gr})} & 0 & \dots & \dots & 0 & a_N^{(\mathrm{ng})} \end{pmatrix} \tag{19}$$

with N the number of observations and M the number of unknown gravity filed parameters. In the absence of noise other than a bias, the vector on the left-hand side of Eq. (18) differs from that on the right-hand side by a constant. In order to remove such a difference, it is enough to subtract the mean value from both vectors. This is the idea behind the *bias-free observation equations*:

$$\mathbf{BAx} = \mathbf{Bd}, \tag{20}$$

where the matrix **B** is such that its application to a (data) vector subtracts the mean within a given interval; in practice, these intervals are set equal to those for which the accelerometer scale factor corrections are computed. Obviously, the matrix **B** can be represented explicitly as follows:

$$\mathbf{B} = \begin{pmatrix} 1-\frac{1}{N_1} & -\frac{1}{N_1} & \dots & -\frac{1}{N_1} & & 0 & \dots & \dots & 0 \\ -\frac{1}{N_1} & 1-\frac{1}{N_1} & & -\frac{1}{N_1} & & 0 & \dots & \dots & 0 \\ & & \ddots & & & & & & \\ -\frac{1}{N_1} & \dots & & 1-\frac{1}{N_1} & & 0 & \dots & \dots & 0 \\ & & & & \ddots & & & & \\ & & & & & \ddots & & & \\ 0 & \dots & \dots & 0 & & 1-\frac{1}{N_n} & -\frac{1}{N_n} & \dots & -\frac{1}{N_n} \\ 0 & \dots & \dots & 0 & & -\frac{1}{N_n} & 1-\frac{1}{N_n} & & -\frac{1}{N_n} \\ & & & & & & & \ddots & \\ 0 & \dots & \dots & 0 & & -\frac{1}{N_n} & \dots & & 1-\frac{1}{N_n} \end{pmatrix}, \tag{21}$$

where N_1, N_2,...,N_n is the number of observations falling into the interval 1, 2,... n.

2.8 Normal equations and computation of the Earth's gravity field model

Let the data covariance matrix be $\mathbf{C_d}$, whereas the a priori covariance matrix of the solution be $\mathbf{C_r}$. In practice, the part

of the matrix $\mathbf{C_r}$ that corresponds to the spherical harmonic coefficients is taken over from the known covariance matrix of the EGM96 model. Due to that, we are able to produce a combined solution that fully exploits a priori information from the GM96 model. The a priori covariances of the other unknowns are assumed to be large (the corresponding elements in the matrix $\mathbf{C_r^{-1}}$ are set equal to zero). Furthermore, the explicit specification of the matrix $\mathbf{C_d}$ is discussed in Sect. 2.9.

The statistically optimal solution $\hat{\mathbf{x}}$ of the system of observation Eq. (20) can be found by solving the system of normal equations:

$$\hat{\mathbf{x}} = \mathbf{N}^{-1}\mathbf{A}^T\mathbf{B}\mathbf{C}_\mathbf{d}^{-1}\mathbf{B}\mathbf{d}, \tag{22}$$

where $\mathbf{N}$ is the normal matrix:

$$\mathbf{N} = \mathbf{A}^{\mathrm{T}}\mathbf{B}\mathbf{C}_\mathbf{d}^{-1}\mathbf{B}\mathbf{A} + \alpha\mathbf{C}_\mathbf{r}^{-1}, \tag{23}$$

and α a coefficient to be found empirically. We have introduced it in order to account for a possibility that one or both of the matrices $\mathbf{C_d}$ and $\mathbf{C_r}$ are known up to a constant factor. Hereafter the coefficient α will be referred to as the "regularization parameter" because it is similar to the regularization parameter in the Tikhonov regularization concept (Tikhonov and Arsenin 1977). For the data set under consideration, the optimal α has been found to be 0.03; for more details, see Sect. 3.2.

An efficient way to solve the system of normal equations is the pre-conditioned conjugate-gradient method (PCCG) (Hestenes and Stiefel 1952), as it was proposed in the context of global gravity field modeling by Schuh (1996). An advantage of this method is that it does not require an explicit assembly of the normal matrix: it is enough to have a procedure for multiplication of the normal matrix with a given vector. Obviously, this procedure can be split into several sub-procedures, each of which multiplies one of the matrices mentioned in Eq. (23) (namely, $\mathbf{A}^{\mathrm{T}}$, $\mathbf{B}$, $\mathbf{C_d^{-1}}$, $\mathbf{A}$, and $\mathbf{C_r^{-1}}$) to a vector. Matrices $\mathbf{B}$ and $\mathbf{C_r^{-1}}$ can be multiplied to vector in a straightforward manner, whereas application of matrices $\mathbf{A}^{\mathrm{T}}$ and $\mathbf{A}$ to a vector can be implemented with fast co-synthesis and fast synthesis algorithms, respectively (Ditmar et al. 2003; Ditmar and van Eck van der Sluijs 2004). Finally, an efficient implementation of the multiplication of the matrix $\mathbf{C_d^{-1}}$ to a vector is dependent on the noise model; this issue is discussed in more details below.

The convergence rate of the PCCG method depends on the selection of the pre-conditioner (a matrix that approximates the true normal matrix). In the context of satellite accelerations, this issue has been extensively discussed by Ditmar and van Eck van der Sluijs (2004). The only real new feature in the currently implemented procedure is the presence of additional unknown parameters (accelerometer scale factors). The corresponding extension of the pre-conditioner has been done by the explicit computation of the diagonal elements related to the additional parameters and setting all other elements equal to zero.

2.9 Noise model

An important aspect of the data processing is a proper stochastic description of noise in the data. The noise model we use is more general than the one proposed by Ditmar and van Eck van der Sluijs (2004) because a non-stationary of noise can be taken into account. To begin with, assume that the data series is uninterrupted. According to Eq. (1), derivation of the observed satellite accelerations $\mathbf{a^{(obs)}}$ from kinematically determined satellite positions $\mathbf{y^{(kin)}}$ in the CRF can be written in the matrix notation as:

$$\mathbf{a^{(obs)}} = \mathbf{D}\mathbf{y^{(kin)}}, \tag{24}$$

where $\mathbf{D}$ is the matrix of the double numerical differentiation with the three-point scheme; for each observational component, the corresponding fragment of this matrix is as follows:

$$\mathbf{D} = \frac{1}{(\Delta t)^2}\begin{pmatrix} 1 & -2 & 1 & & \\ & \ddots & \ddots & \ddots & \\ & & 1 & -2 & 1 \end{pmatrix} \tag{25}$$

By taking the rotation to/from the CRF into account, the following expression can be written for the data covariance matrix $\mathbf{C_d}$:

$$\mathbf{C_d} = \mathbf{R_{CRF\to LORF}}\,\mathbf{D}\,\mathbf{R_{LORF\to CRF}}\,\mathbf{C_y^{(LORF)}}\,\mathbf{R_{CRF\to LORF}}\,\mathbf{D}^{\mathrm{T}}\,\mathbf{R_{LORF\to CRF}}, \tag{26}$$

where $\mathbf{C_y^{(LORF)}}$ is the covariance matrix of kinematically determined positions [it consists of 3×3 blocks $\mathbf{Q_j^{(LORF)}}$ which are defined by Eq. (5)]; and $\mathbf{R_{CRF\to LORF}}$ and $\mathbf{R_{LORF\to CRF}}$ are rotation matrices (the names are self-explaining). The rotation matrices also consist of blocks, each of which is a 3×3 rotation matrix for a given epoch.

Unfortunately, the definition of the covariance matrix (26), even if formally correct, leads in practice to models of poor quality. This can be understood as follows. Assume that noise in kinematically-determined satellite positions is stationary and non-correlated (the matrix $\mathbf{C_y}$ is proportional to the unit one). The double differentiation of a time series is approximately equivalent in the Fourier domain to multiplication of its spectrum by the factor $-\omega^2$, where ω is the cyclic frequency. Hence, the double differentiation of positions contaminated by white noise would make the noise power spectral density proportional to ω^4. The optimal data weighting procedure compensates such an increase by assigning to data the weights which are inversely proportional to the power spectral density. It means that the signal at high frequencies gets low weights, whereas weights at low frequencies increase almost infinitely as the frequency approach zero! In other words, the formal data weighting suggests that orbit-derived accelerations are extremely accurate at low frequencies. Of course, such an assumption is not realistic. There are a number of reasons for accelerations to be inaccurate at low frequencies such as accelerometer noise and noise in the reduced-dynamic orbit. Therefore, it makes sense to update the formal data weighting scheme so that data weights at low frequencies are kept limited. It can be shown (Ditmar and

van Eck van der Sluijs 2004) that the factor $-\omega^2$ turns into $-[\omega^2 + (\epsilon/\Delta t)^2]$ if the double differentiation matrix $\mathbf{D}$ in the expression for the data covariance matrix (26) is replaced with its regularized version $\tilde{\mathbf{D}}$:

$$\tilde{\mathbf{D}} = \frac{1}{(\Delta t)^2} \begin{pmatrix} -1 & 2+\epsilon^2 & -1 & & \\ & \ddots & \ddots & \ddots & \\ & & -1 & 2+\epsilon^2 & -1 \end{pmatrix}, \tag{27}$$

where the sign of all the entries is changed in order to make the matrix $\tilde{\mathbf{D}}$ positive-definite [this can be done with impunity because the matrix $\mathbf{D}$ appears in Eq. (26) twice].

To clarify the influence of the parameter ϵ on data weighting, we find it important to mention that the matrix $\tilde{\mathbf{D}}$ has a pseudo-inverse matrix $\mathbf{F}$ in the following sense:

$$\left(\tilde{\mathbf{D}}\tilde{\mathbf{D}}^{\mathrm{T}}\right)^{-1} \approx \mathbf{F}^2 \tag{28}$$

(Ditmar and van Eck van der Sluijs 2004). The matrix $\mathbf{F}$ is a Toeplitz one, i.e., its application to a vector is nothing but filtering this vector. The explicit expression for the filter coefficients f_j is:

$$f_j = \frac{\Delta t\, \tau}{2}\, \mathrm{e}^{-(|j|\Delta t/\tau)}, \tag{29}$$

where $\tau = \Delta t/\epsilon$. Obviously, the filter represented by the matrix $\mathbf{F}$ is a low-pass filter with a half-width τ. The extreme case $\tau \to \infty$ ($\epsilon \to 0$) corresponds to the matrix $\tilde{\mathbf{D}}$ with no regularization, i.e., to purely non-correlated noise in *positions*. The extreme case $\tau \to 0$ ($\epsilon \to \infty$) makes the matrix $\tilde{\mathbf{D}}$ proportional to the unit one (with two extra columns filled with zeroes):

$$\tilde{\mathbf{D}} \xrightarrow[\tau\to 0]{} \frac{1}{\tau^2} \begin{pmatrix} 0 & 1 & 0 & & \\ & \ddots & \ddots & \ddots & \\ & & 0 & 1 & 0 \end{pmatrix}. \tag{30}$$

This case corresponds to non-correlated noise in *accelerations*. In processing the CHAMP data under consideration, the parameter τ has been set equal to 60 s ($\epsilon^2 = 0.25$); see Sect. 3.2 for more details.

Numerical examples show (Ditmar and van Eck van der Sluijs 2004) that for a sufficiently short filter (for example, $\tau \leq 600$ s), the influence of rotation to/from the CRF in the covariance matrix of Eq. (26) becomes negligible. For the extreme case $\tau \to 0$, this is obvious. Thus, the final expression for the data noise covariance matrix $\mathbf{C_d}$ can be written as follows:

$$\mathbf{C_d} = \tilde{\mathbf{D}}\, \mathbf{C}_{\mathbf{y}}^{(\mathbf{LORF})}\, \tilde{\mathbf{D}}^{\mathrm{T}}. \tag{31}$$

In case of a data set with gaps, the noise covariance matrix can be obtained from that of Eq. (31) by removing rows and columns which correspond to discarded epochs (Ditmar and van Eck van der Sluijs 2004). The matrix $\mathbf{C}_{\mathbf{y}}^{(\mathbf{LORF})}$, which describes the position accuracy, is assumed to be uninterrupted in any case.

In order to apply the inverse covariance matrix $\mathbf{C_d}^{-1}$ to a vector efficiently and accurately, we make use of a low-level PCCG scheme (Ditmar and van Eck van der Sluijs 2004; Ditmar et al. 2004). The accuracy of this scheme depends on how accurately the covariance matrix $\mathbf{C_d}$ can be multiplied with a vector. Fortunately, this is not a problem, even if data contain gaps (Ditmar and van Eck van der Sluijs 2004). The numerical efficiency is controlled by the pre-conditioning operation, where the matrix $\mathbf{C_d}^{-1}$ has to be applied to a vector approximately. To make the pre-conditioning efficient, the pre-conditioner should deviate from the true matrix as little as possible. We have found that the inverse covariance matrix approximated as

$$\mathbf{C_d}^{-1} \equiv \mathbf{F}\, \left(\mathbf{C}_{\mathbf{y}}^{(\mathbf{LORF})}\right)^{-1}\, \mathbf{F} \tag{32}$$

can be used as an extremely efficient pre-conditioner (the number of PCCG iterations typically remains in the range of 10–20).

It is worth adding that Eq. (32) is, strictly speaking, not correct from the point of view of linear algebra because matrices $\mathbf{F}$ and $\mathbf{C}_{\mathbf{y}}^{(\mathbf{LORF})}$ have different sizes. If the data series is uninterrupted, the number of rows/columns in the latter matrix exceeds that in the former one by 2; for an interrupted data set, this difference is even larger. There are, however, no reasons to worry about this fact because the pre-conditioning is an approximate operation anyway. In practice, it is enough just to truncate "spare" rows and columns of matrix $\mathbf{C}_{\mathbf{y}}^{(\mathbf{LORF})}$ in Eq. (32) (in case of an uninterrupted data set, these are the first and the last column and row).

3 Results

3.1 The optimal gravity field model

Processing of the CHAMP data as outlined above has resulted in a new Earth's gravity field model complete up to degree and order 70, which was called DEOS_CHAMP-01C_70. The key features of the data set and of the processing strategy exploited are listed in Table 3. The potential coefficients and other parameters comprising the model are available at the web-page http://icgem.gfz-potsdam.de/ICGEM/shms/deos_champ-01c.gfc. Furthermore, the necessary information to supplement the model coefficients is given in Table 4.

Figure 2 shows the difference between the DEOS_CHAMP-01C_70 model on the one hand and two other models – EGM96 and EIGEN-GRACE01S–on the other hand, expressed in terms of geoid heights; the latter two models are truncated at degree 70. Thereafter, we consider the EIGEN-GRACE01S model (http://www.gfz-potsdam.de/pb1/op/grace/results/index_RESULTS.html) as the "ground truth" because its accuracy is much higher than that of any model derived from CHAMP data (except for, may be, degree 2). It is noteworthy, that our model is much closer to the EIGEN-GRACE01S model than to the EGM96, even though some information in our model definitely originates from the EGM96 model (this is due to the fact that the EGM96 model is used as the reference one, whereas the EGM96 covariance

Table 3 The data set and processing strategy used in the computation of the DEOS_CHAMP-01C_70 model

Time interval covered by the observations	March 10, 2002 to January 25, 2003
Number of three-component accelerations used	666,581
Reference static gravity field model	EGM96
Tides corrected for	Astronomic (Moon and Sun), solid Earth, and ocean
Numerical ephemerides (moon and sun)	DE405
Love numbers in solid Earth tides modeling	PREM
Model of the ocean tides	GOT00.2
Load love numbers	IERS conventions
Maximum degree and order solved for	70
Parameter τ in the noise model	60 s
Regularization matrix	Covariance matrix of the EGM96 model
Regularization parameter (α)	0.03
Time intervals defined for an estimation of residual accelerometer scale factors and elimination of a bias	10 days

Table 4 Necessary information to supplement the spherical harmonic coefficients of the DEOS_CHAMP-01C_70 model

Semi-major axis of the reference ellipsoid (a)	6,378,136.3 m
GM factor	$3.986004415 \times 10^{14}$ m^3/s^2
Tidal system	Tide-free
Reference epoch (middle of the observation interval)	16 August, 2002
Reference frame	ITRF2000 (IGS00 realization)

matrix is utilized as the regularization matrix). Especially large deviations between the DEOS_CHAMP-01C_70 and EGM96 models are observed in remote areas: Antarctica, Amazon river basis, and Himalayas, i.e., in the areas which were hardly studied at the time when the EGM96 model was assembled (see Fig. 2a). It is interesting that the same geographical areas show also a relatively big difference between the DEOS_CHAMP-01C_70 and the EIGEN-GRACE01S models, especially at high spatial frequencies. This is an evidence of a relatively low accuracy of our model in these areas. Such a behavior is not surprising because recovery of a gravity field from CHAMP data inevitably introduces some smoothing. As long as the residual gravity field in the remote areas is large, the errors caused by smoothing are also more prominent.

Figure 3 offers other ways to compare the DEOS_CHAMP-01C_70 model with EIGEN-GRACE01S: as cumulative geoid height differences and as geoid height differences per degree. These differences are remarkably small. In particular, the cumulative geoid height difference stays below 1 cm up to degree 20 and below 10 cm up to degree 60.

Furthermore, we have compared the DEOS_CHAMP-01C_70 model with two other recently distributed models that have been derived from CHAMP data: EIGEN-3p (Reigber et al. 2005a) and ITG-CHAMP01E (Mayer Gürr et al. 2005). For all the models, the difference with respect to the EIGEN-GRACE01S has been computed in terms of geoid heights; all the models being truncated at degree 70 (Table 5). To obtain the geoid height differences, we have computed the residual potential on a regular grid at the reference sphere with radius of 6,371 km, and then divided it by 9.8 m/s^2 . It goes without saying that the area weights are applied when computing the RMS differences. It is worth noticing that some authors set the radius of the reference sphere equal to the equatorial radius of the Earth. In that case, the geoid height differences may decrease by a few percents. To make the comparison more comprehensive, the differences are presented also in terms of cumulative geoid heights (Fig. 4).

Another way to compare models is to use them for a numerical integration of a satellite orbit. Such a test was kindly done for us by P. Visser (DEOS, Delft Technical University). In this test, a high-quality reduced-dynamic orbit solution (van den IJssel et al. 2003) was used as pseudo-observations in a purely dynamic orbit determination. These pseudo-observations are the inertial X, Y and Z coordinates, sampled at 60-s time interval in daily batches (i.e., 1,441 points per day). The data period covers DOY 140-150 in 2001, which is the period used in the CHAMP IGS LEO orbit comparison campaign (http://nng.esoc.esa.de/gps/CH_campaign.html). A dynamic orbit is computed per day. In total, 13 parameters are estimated: (1) initial state vector (6 parameters); (2) along-track and cross-track accelerometer bias and scale factor (4 parameters); (3) radial bias + 1 cycle-per-revolution sine/cosine (3 parameters). Three models have been compared in this way: EGM96, EIGEN-3p, and DEOS_CHAMP-01C_70 (Table 6).

From the comparisons, one can see that DEOS_CHAMP-01C_70 shows less geoid height errors at large degrees than EIGEN-3p model. This can be explained by the fact that the EIGEN-3p model, unlike the DEOS_CHAMP-01C_70, was computed independently from EGM96. At intermediate degrees, the EIGEN-3p model is more accurate. Also, the orbit integration based on the EIGEN-3p model demonstrates a higher accuracy. This is not very surprising because the EIGEN-3p model used more data than our model (3 year vs. 322 days). At low degrees, DEOS_CHAMP-01C_70 seems to have smaller errors in terms of geoid heights than the EIGEN-3p model. The probable explanation is a proper frequency-dependent data weighting we apply (see also a discussion in Sect. 4). The same explanation can probably be used to explain differences between the DEOS_CHAMP-01C_70 and the ITG-CHAMP01E models.

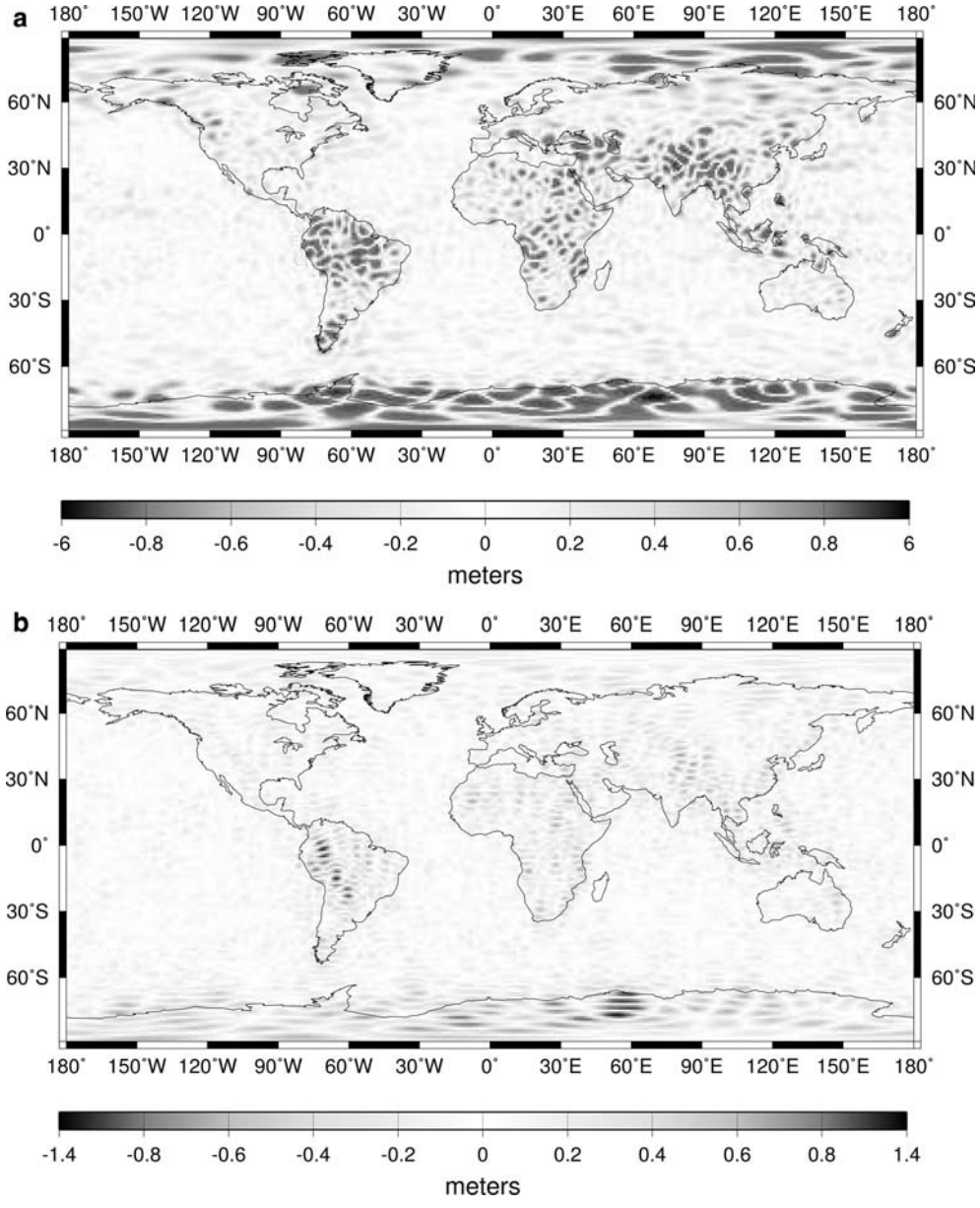

Fig. 2 Geoid height difference between the DEOS_CHAMP-01C_70 model and **a** EGM96 (the rms difference is 0.342 m, the maximum difference is 5.61 m); **b** EIGEN-GRACE01S (the rms difference is 0.142 m, the maximum difference is 1.29 m)

Table 5 Difference between various gravity field models and the EIGEN-GRACE01S model in terms of geoid heights (a truncation at degree 70 is applied)

Model	RMS geoid height difference (m)	Maximum geoid height difference (m)
EGM96	0.36	5.92
EIGEN-3p	0.30	2.98
ITG-CHAMP01E	0.18	1.69
DEOS_CHAMP-01C_70	0.14	1.29

3.2 Dependence of the model on empirically determined parameters

A number of parameters have been chosen empirically when computing the gravity field model DEOS_CHAMP-01C_70. We found that two of them influence the resulting model mostly: (1) the parameter τ in the data weighting scheme and (2) the regularization parameter α. In order to choose these parameters optimally, a series of models has been produced, each of which was compared with the EIGEN-GRACE01S.

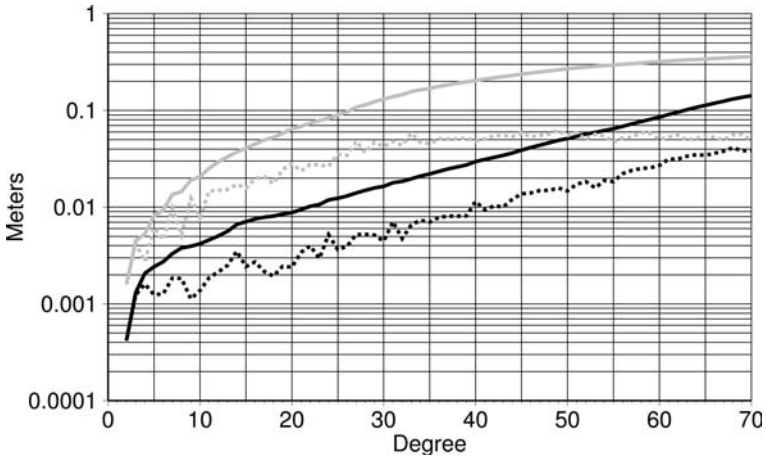

Fig. 3 Comparison of the DEOS_CHAMP-01C_70 model with EIGEN-GRACE01S (in *black*): cumulative geoid height differences (*solid line*) and geoid height difference per degree (*dotted line*). Geoid height differences between EGM96 and EIGEN-GRACE01S models (cumulative and per degree) are shown for a reference (*grey lines*)

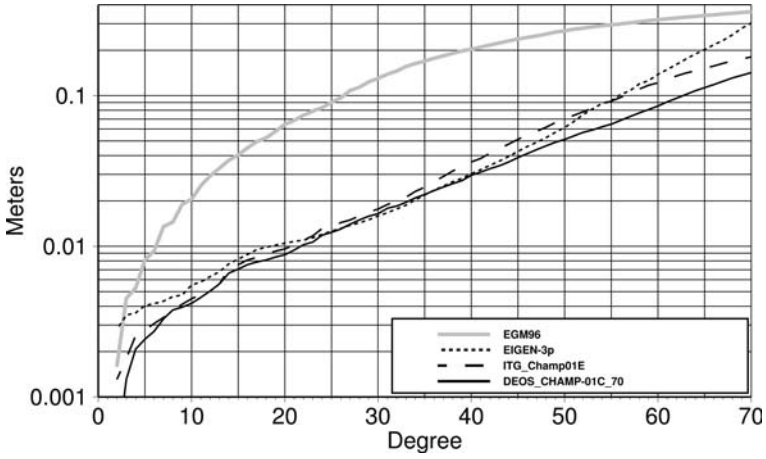

Fig. 4 Comparison of various CHAMP-based models in terms of cumulative geoid height differences with respect to EIGEN-GRACE01S; EGM96 model is included as a reference. Degree 1 terms in the EIGEN-3p model are ignored

Table 6 Performance of different gravity field models in purely dynamic orbit determination of CHAMP satellite

Gravity field model	Inertial coordinate	Number epochs	Mean fit (cm)	Rms fit (cm)
	X	15851	2.74	173.14
EGM96	Y	15851	−4.05	117.36
	Z	15851	0.76	128.96
	X	15851	−2.65	22.87
EIGEN-3p	Y	15851	4.06	17.18
	Z	15851	0.01	26.90
	X	15851	−2.50	31.96
DEOS_CHAMP-01C_70	Y	15851	3.77	25.42
	Z	15851	−0.08	40.67

Figure 5 shows the cumulative geoid height differences for three values of the parameter τ: 60 s, 180 s, and $\tau \to 0$. The latter case corresponds to the matrix $\tilde{\mathbf{D}}$ set equal to $1/(\Delta t)^2\mathbf{I}$, where $\mathbf{I}$ is the unit matrix [possibly, with some extra columns filled with zeroes, cf. Eq. (30)]; in other words, noise in accelerations is assumed to be non-correlated in time. Importantly, each of the shown curves corresponds to the optimally chosen regularization parameter α. RMS and maximum geoid height differences with respect to the EIGEN-GRACE01S model for τ equal to 0, 60, 180, 600, and 1,200 s are given in Table 7. One can seen that the model quality remains relatively high for short τ (including $\tau \to 0$) but degrades for larger τ.

Furthermore, Table 7 shows how the model depends on the regularization parameter, provided that τ is optimal (60 s). The comparison in terms of cumulative geoid height

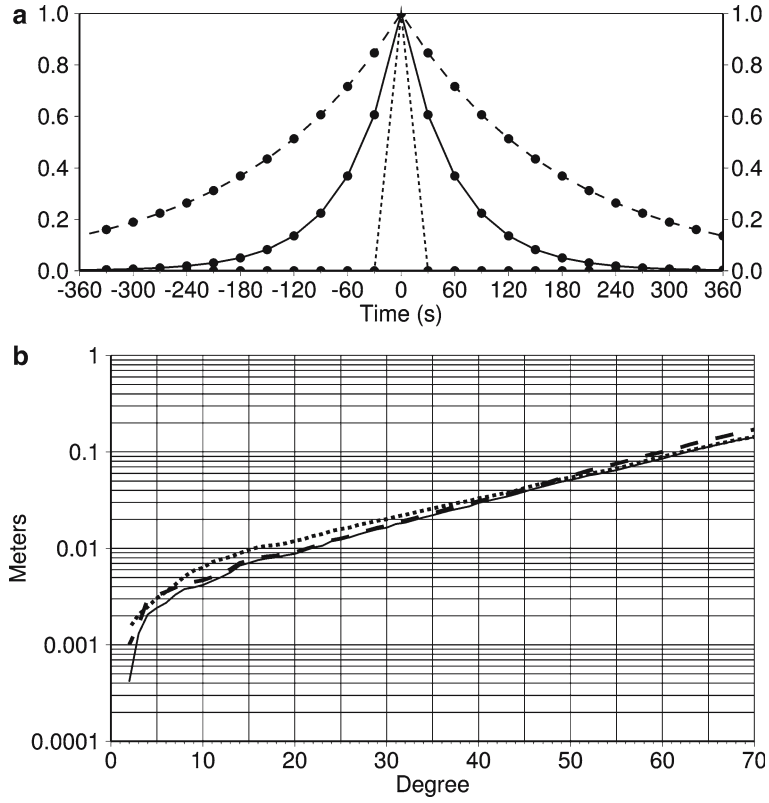

Fig. 5 Dependence of the gravity field model on the parameter τ in the data weighting scheme (the regularization is optimal): **a** The (normalized) filter that approximates the matrix $\tilde{\mathbf{D}}^{-1}$ [see Eq. (28)], in the time domain; **b** cumulative geoid height difference between the computed gravity field models and EIGEN-GRACE01S. The *dotted, solid*, and *dashed lines* correspond to the data weighting with $\tau \to 0$, with $\tau = 60$ s (the optimal model), and with $\tau = 180$ s, respectively

Table 7 Dependence of the model quality on the empirically determined parameters. The table shows rms and maximum geoid height differences with respect to to EIGEN-GRACE01S model truncated at degree 70

Parameter τ in the noise model (s)	Regularization parameter (α)	RMS geoid height difference (m)	Maximum geoid height difference (m)
0	(Optimal)	0.143	1.35
60	0.03 (optimal)	0.142	1.29
180	(Optimal)	0.171	1.99
600	(Optimal)	0.254	2.38
1,200	(Optimal)	0.280	2.81
60	0.003	0.199	1.24
60	0.01	0.160	1.06
60	0.1	0.148	1.51
60	0.3	0.170	1.84

differences is presented in Fig. 6. One can see that modest deviations of the regularization parameter from the optimal value do not distort the model significantly, whereas larger deviations (say, more than three times relatively to the optimal values) can make the model rather inaccurate.

3.3 Accelerometer scale factors

As was explained in Sect. 2.7, the gravity field model has been computed simultaneously with residual accelerometer scale factors $c_k(j)$. We found, however, that the estimated scale factors are rather sensitive to the data processing strategy exploited, especially at the radial component. An example of such a sensitivity is given in Fig. 7 which shows the estimated scale factors for 3 values of parameter τ (0, 60, and 180 s). Furthermore, another selection of time intervals at which the scale factors are assessed (say, once per day) can make these estimations totally unreasonable. Thus, it is not advisable to use the proposed data processing technique for computation of accelerometer scale factors. It is important to notice, however, that variations of these scale factors practically do not influence the gravity field model. In the context of gravity field studies, such a behavior can be considered as an asset rather than a drawback.

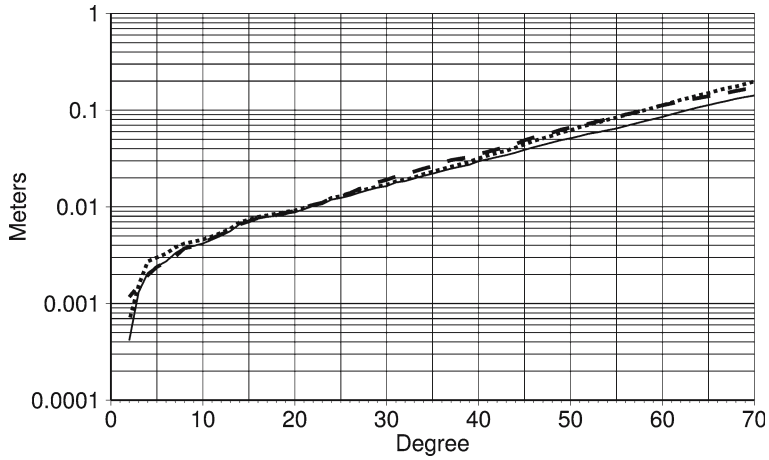

Fig. 6 Dependence of the gravity field model on the regularization parameter α ($\tau = 60$ s): cumulative geoid height difference between the computed models and EIGEN-GRACE01S. The *dotted, solid*, and *dashed line* correspond to the parameter α equal to 0.003, 0.03, and 0.3, respectively

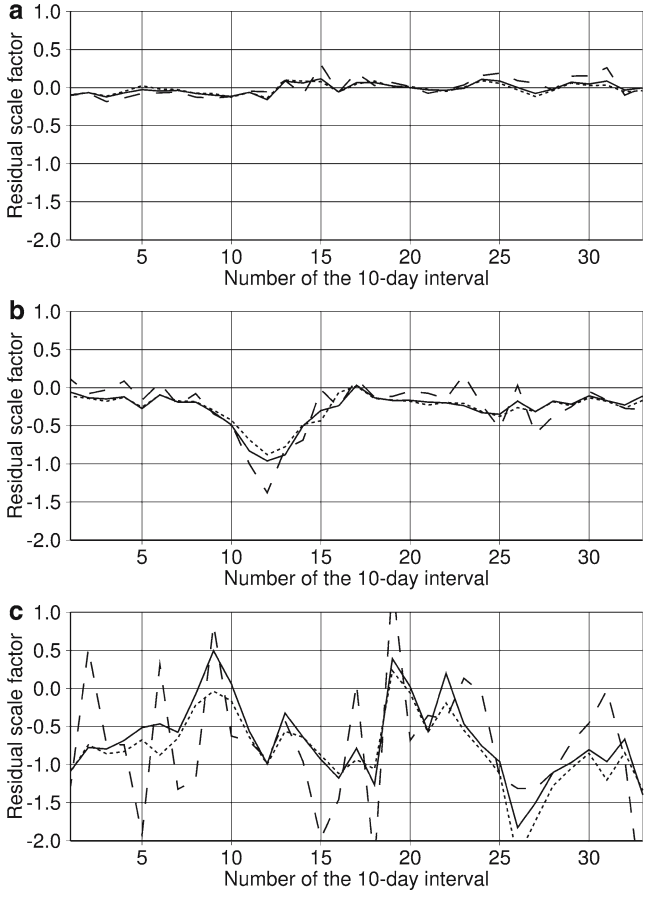

Fig. 7 Sensitivity of the computed residual accelerometer scale factors to the data weighting scheme (**a** along-track component; **b** cross-track component; **c** radial component). The *dotted, solid*, and *dashed lines* correspond to the parameters τ set equal to 0, 60 s (the optimal model), and 180 s, respectively

4 Discussion and conclusions

A new gravity field model DEOS_CHAMP-01C_70 has been computed from observed accelerations of the CHAMP satellite, according to the computational scheme proposed by Ditmar and van Eck van der Sluijs (2004). This model can successfully compete with other CHAMP-based models published recently. To a large extent, this is due to the fact that our functional model exploits satellite accelerations rather than positions (or velocities) of the satellite. Then, even without putting much efforts into frequency-dependent data weighting, we are able to produce a high-quality model, which is insensitive to low-frequency noise. In particular, the errors related to non-gravitational accelerations (e.g., due to inaccurately determined accelerometer scale factors) fall mostly in the low-frequency band and therefore do not propagate into the model. The situation is different when, for example, the approach based on the integration of variational equations is applied. In that case, the absence of a frequency-dependent data weighting means that noise is assumed to be white in terms of satellite positions. This corresponds to the assumption that noise in accelerations increases proportionally to the frequency squared. Thus, data at lowest frequencies are weighted extremely high, and even minor errors at those frequency can distort the model noticeably. A poor quality of our models produced with a too large parameter τ serves a good illustration of how over-weighted low-frequency information can deteriorate a model.

It is worth noticing that an important stage of data processing is data screening. In this way, large errors in the kinematic orbit can be eliminated. Of course, the data screening should be done with caution. A too strict threshold in data screening can remove not only outliers but also good measurements in remote geographic areas, where the reference model is especially inaccurate (e.g., in Antarctica). To prove that this does not happen in our case, we have plotted the geographical location of the epochs discarded (Fig. 8). One can see that the eliminated points are evenly distributed over the globe; a correlation with remote areas is not observed.

The functional model we exploit is defined in the LORF. This offers an easy way to exclude the radial component of satellite accelerations from gravity field modeling. At the first glance, this is an attractive option because this component

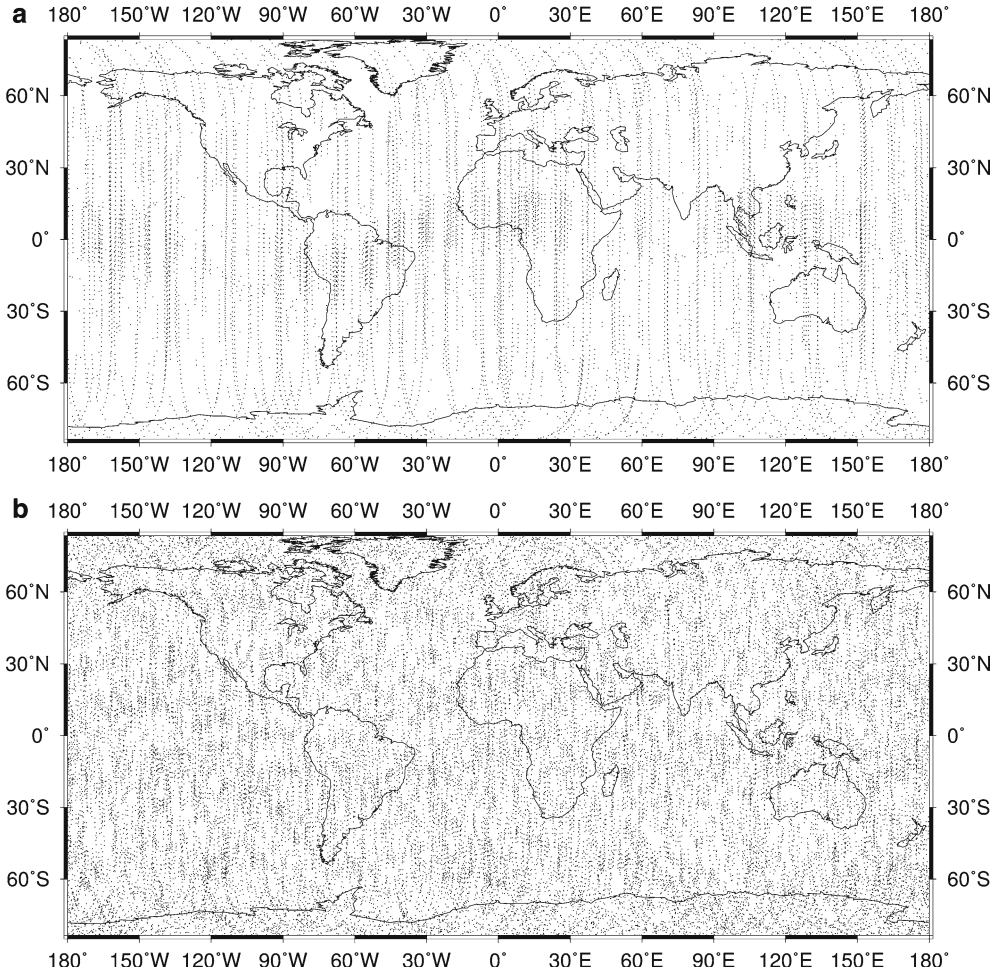

Fig. 8 Geographical location of the epochs discarded (a) because the kinematic orbit deviated by more than 50 cm from the reduced-dynamic one and (b) because a discontinuity in the kinematic orbit has been revealed as explained in section 2.4

suffers from systematic distortions caused by a poor performance of the corresponding accelerometer axis. On the other hand, the exclusion of the radial component reduces the amount of input data for gravity field modeling. Even though the radial component contains less information than the horizontal ones (this is an intrinsic property of GPS data reflected also in the stochastic models), a gravity field model obtained without this component can be somewhat worse. To see which of the two effects dominates, we have repeated the data processing as outlined above, but using the along-track and cross-track acceleration component only. The quality of the resulting model can be evaluated with Fig. 9. One can see that at the low degrees elimination of the radial component improves the gravity field model. At higher degrees, however, the alternative model is slightly worse. The rms geoid height difference between the alternative model and the EIGEN-GRACE01S is 0.144 m, whereas the maximum difference is 1.34 m (compare this with results of 3-component data processing: 0.142 and 1.29 m, respectively). Thus, distortions of the radial accelerations caused by the accelerometer do not play a significant role. This is one more evidence that the proposed data processing scheme is not sensitive to accelerometer errors.

Another issue to be discussed is the accuracy of the EIGEN-GRACE01S model, which is used as the ground truth throughout the paper. This model is based on only 39 days of GRACE data. One may expect, therefore, that at least a part of the differences between a CHAMP-based and the EIGEN-GRACE01S models can be explained by an inaccuracy of the EIGEN-GRACE01S model itself. In order to clarify this issue, we have compared also the DEOS_CHAMP-01C_70 model with EIGEN-CG01C (Reigber et al. 2005b). The latter is definitely more accurate than EIGEN-GRACE01S because it is based, in particular, on 200 days of GRACE data. Nevertheless, only negligible changes could be observed in geoid height differences. In particular, the rms value has decreased to 0.141 m and the maximum value has increased to 1.30 m.

It is, naturally, annoying that we have to rely on a GRACE-derived model in order to determine optimally some of the parameters in the data processing scheme. For this reason, we work on a further improvement of the processing methodology so that it becomes totally independent of the "ground

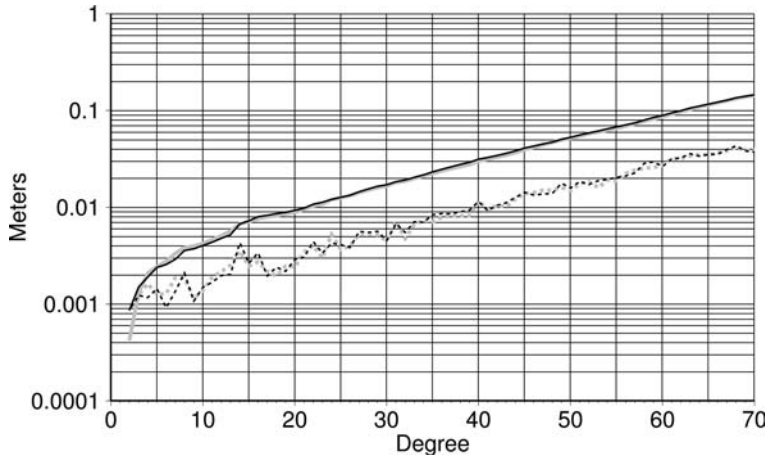

Fig. 9 Processing of horizontal acceleration components only: comparison of the resulting gravity field model with EIGEN-GRACE01S (in black): cumulative geoid height differences (solid line) and geoid height difference per degree (dotted line). Geoid height differences between DEOS_CHAMP-01C_70 and EIGEN-GRACE01S models (cumulative and per degree) are shown for a reference (grey lines)

truth." In particular, we study options to improve the stochastic model of data noise. Until now, we relied on the noise estimations that are distributed together with the kinematic orbit in the form of a 3×3 covariance matrix per epoch. There are, however, reasons to assume that these estimations are incomplete and/or inaccurate. The first evidence is a "strange" behavior of the outlier detection procedure, which screens out only 4% data, though at least 50% must be screened out for purely statistical reasons, even if there were no outliers at all. The second evidence is a low value of the optimal regularization parameter (0.03). It is important to note that just a scaling of the provided covariance matrices is not enough to improve the stochastic noise model. It will be necessary, at least, to estimate also the dependence of noise on frequency. A better knowledge of data noise will allow us to make the data screening procedure justified better and to find the optimal parameter τ in the data weighting procedure. Furthermore, it will make the introduction of the "regularization" parameter α not necessary: it will be close to 1 (provided that the covariance matrix of the EGM96 model is sufficiently accurate).

It will also be important to increase the maximum degree of the model obtained. The maximum degree of 70, which has been used so far, is dictated by the fact that the complete covariance matrix of the EGM96 model exists only up to this degree. It will be, therefore, important to find the optimal way to specify the regularization matrix when information about stochastic properties of the reference model is incomplete.

We have not studied yet if the proposed technique can be adjusted to provide not only a gravity field model, but also accurate estimations of accelerometer scale factors. It is likely that the goal can be reached by switching from the LORF to the Satellite Body Frame (SBF) in the definition of the functional model. Then, scale factors $c_{k(j)}$ in Eq. (17) could be associated with accelerometer axes exactly rather than approximately. Of course, the question is if the usage of another frame for the definition of the functional model may influence the gravity field model itself. In our opinion, this is unlikely (it could happen if our model were sensitive to inaccuracies in accelerometer scale factors, but this is not the case). Furthermore, we do not expect that such a re-definition of the functional model will change the numerical performance of the procedure for computing the (residual) spherical harmonic coefficients. Differences between the LORF and the SBF are as small as a fraction of degree and, therefore, the dominant block-diagonal structure of the normal matrix is preserved so that the block-diagonal pre-conditioner we use must not loose its efficiency.

Acknowledgements We thank D. Švehla and M. Rothacher (Technical University Munich) for providing us with kinematic and reduced-dynamic orbits of the CHAMP satellite. We are thankful to P. Visser (DEOS, Delft Technical University) for doing the orbit integration test for us. Furthermore, we are extremely grateful to the reviewers of the manuscript: P. Schwintzer, Ch. Reigber, and Ch. Tscherning; their valuable remarks helped us to improve the paper considerably. The computations have been done on the SGI Origin 3800 and SGI Altix 3700 super-computers in the framework of the grant SG-027, which was provided by "Stichting Nationale Computerfaciliteiten" (NCF). The support of NCF is gratefully acknowledged.

References

Ditmar P, Klees R, Kostenko F (2003) Fast and accurate computation of spherical harmonic coefficients from satellite gravity gradiometry data. J Geod 76:690–705

Ditmar P, van Eck van der Sluijs A, Kuznetsov V (2004) Modeling the Earth's gravity field from precise satellite orbit data: the acceleration approach works! (available as http://earth.esa. int/workshops/goce04/participants/81/paper_accelerations.pdf). In: Proceedings of the 2nd international GOCE user workshop, Frascati (Italy), 8-10 March, 2004. European Space Agency

Ditmar P, van Eck van der Sluijs AA (2004) A technique for Earth's gravity field modeling on the basis of satellite accelerations. J Geod 78:12–33

Dziewonski, AM, Anderson DL (1981) Preliminary reference Earth model (PREM). Phys Earth Planet Int 25:297–356

Fengler MJ, Freeden W, Michel V (2004) The Kaiserslautern multiscale geopotential model SWITCH-03 from orbit perturbations of the satellite CHAMP and its comparison to the models EGM96, UCPH2002_02_0.5, EIGEN-1s, and EIGEN-2. Geophys J Int 157(2):499–514

Gerlach C, Földvary L, Švehla D, Gruber T, Wermuth M, Sneeuw N, Frommknecht B, Oberndorfer H, Peters T, Rothacher M, Rummel R, Steigenberger P (2003a) A CHAMP-only gravity field model from kinematic orbits using the energy integral. Geophys Res Lett 30(20):2037. doi: 10.1029/2003GL018025

Gerlach C, Sneeuw N, Visser P, Švehla D (2003b) CHAMP gravity field recovery using the energy balance approach (available as http://www.copernicus.org/EGU/adgeo/2003/1/adg-1-73.pdf). Adv Geosci 1:73–80

Han S-C, Jekeli C, Shum CK (2002) Efficient gravity field recovery using in situ disturbing potential observables from CHAMP. Geophys Res Lett 29(16) 10.129/2002GL015180

Hestenes MR, Stiefel E (1952) Methods of conjugate gradients for solving linear systems. J Res Nat Bureau Stand 49:409–436

Howe E, Stenseng L, Tscherning CC (2003) Analysis of one month of CHAMP state vector and accelerometer data for the recovery of the gravity potential (available as http://www.copernicus.org/EGU/adgeo/2003/1/adg-1-1.pdf). Adv Geosci 1:1–4

Ilk K-H (1984) On the analysis of satellite-to-satellite tracking data. In: Proceedings of the International symposium on space techniques for geodesy. Sopron, Hungary 9–13 July 1984, pp 59–74

Ilk KH, Feuchtinger M, Mayer-Ġurr T (2003) Gravity field recovery and validation by analysis of short arcs of a satellite-to-satellite tracking experiment as CHAMP and GRACE. In: Proceedings of the IAG symposium G02, IUGG general assembly 2003, Sapporo, Japan

Ilk KH, Mayer-Gürr T, Feuchtinger M (2005) Gravity field recovery by analysis of short arcs of CHAMP. In: Reigber C, Ľuhr H, Schwintzer P, Wickert J, (eds) Earth observation with CHAMP, results from three years in orbit, Springer, Berlin Heidelberg New York, pp 127–132

Lambeck K Geophysical geodesy: the slow deformations of the Earth. Clarendon, Oxford, 1988

Lemoine FG, Kenyon SC, Factor JK, Trimmer RG, Pavlis NK, Chinn DS, Cox CM, Klosko SM, Luthcke SB, Torrence MH, Wang YM, Williamson RG, Pavlis EC, Rapp RH, Olson TR (1998) The development of the joint NASA GSFC and the National Imagery and Mapping Agency (NIMA) geopotential model EGM96. NASA/TP-1998-206861. NASA GSFC, Greenbelt, MD

Mayer-Ġurr T, Ilk KH, Eicker A, Feuchtinger M (2005) ITG-CHAMP01: A CHAMP gravitiy field model from short kinematical arcs of a one-year observation period. J Geod 78:462–480

McCarthy DD, Petit G (2004) IERS Conventions (2003) (IERS Technical Note; 32). Verlag des Bundesamts fŕ Kartographie und Geodäsie, Frankfurt am Main

O'Keefe JA (1957) An application of Jacobi's integral to the motion of an Earth satellite. The Astronomi J 62(1252):265–266

Ray RD (1999) A global ocean tide model from TOPEX/POSEIDON altimetry: GOT99.2. NASA technical memorandum 209478

Reigber C (1989) Gravity field recovery from satellite tracking data. In: Sansò F, Rummel R (eds) Theory of satellite geodesy and gravity field determination. Lect notes Earth Sci 25:197–234. Springer, Berlin Heidelberg New York

Reigber C, Balmino G, Schwintzer P, Biancale R, Bode A, Lemoine J-M, König R, Loyer S, Neumayer H, Marty J-C, Barthelmes F, Perosanz F, Zhu SY (2002) A high-quality global gravity field model from CHAMP GPS tracking data and accelerometry (EIGEN-1S). Geophys Res Lett 29(14). 10.1029/2002GL015064

Reigber C, Balmino G, Schwintzer P, Biancale R, Bode A, Lemoine J-M, König R, Loyer S, Neumayer H, Marty J-C, Barthelmes F, Perosanz F, Zhu SY (2003a) Global gravity field recovery using solely GPS tracking and accelerometer data from CHAMP. Space Science Reviews, 108(1-2):55–66

Reigber C, Balmino G, Schwintzer P, Biancale R, Bode A, Lemoine J-M, König R., Loyer S, Neumayer H, Marty J-C, Barthelmes F, Perosanz F, Zhu SY (2003b) New global gravity field models from selected CHAMP data sets. In: Reigber C, Lühr H, Schwintzer P (eds) First CHAMP mission results for gravity, magnetic, and atmospheric studies. Springer, Berlin Heidelberg New York, pp 120–127

Reigber C, Bock R, Forste C, Grunwaldt L, Jakowski N, Lühr H, Schwintzer P, Tilgner C (1996) CHAMP phase B executive summary. GFZ, STR96/13, Potsdam

Reigber C, Jochmann H, Wünsch J, Petrovic S, Schwintzer P, Barthelmes F, Neumayer K-H, König R, Förste C, Balmino G, Biancale R, Lemoine J-M, Loyer S, Perosanz F (2005a) Earth gravity field and seasonal variability from CHAMP. In: Reigber C, Lühr H, Schwintzer P, Wickert J (eds) Earth observation with CHAMP – results from three years in orbit, Springer, Berlin Heidelberg New York, pp 25–30

Reigber C, Schwintzer P, Neumayer K-H, Barthelmes F, König R, Förste C, Balmino G, Biancale R, Lemoine J-M, Loyer S, Bruinsma S, Perosanz F, Fayard T (2003c) The CHAMP-only Earth gravity field model EIGEN-2. Adv Space Res 31(8):1883–1888 doi: 10.1016/S0273-1177(03)00162-5

Reigber C, Schwintzer P, Stubenvoll R, Schmidt R, Flechtner F, Meyer U, König R, Neumayer H, Förste C, Barthelmes F, Zhu SY, Balmino G, Biancale R, Lemoine J-M, Meixner H, Raimondo JC (2005b) A high resolution global gravity field model combining CHAMP and GRACE satellite mission and surface gravity data: EIGEN-CG01C. J Geod (accepted)

Reubelt T, Austen G, Grafarend EW (2003a) Harmonic analysis of the Earth's gravitational field by means of semi-continuous ephemerides of a low Earth orbiting GPS-tracked satellite. Case study: CHAMP. J Geod 77:257–278

Reubelt T, Austen G, Grafarend EW (2003b) Space gravity spectroscopy – determination of the Earth's gravitational field by means of Newton interpolated LEO ephemeris. Case studies on dynamic (CHAMP rapid science orbit) and kinematic orbits (available as http://www.copernicus.org/EGU/adgeo/2003/1/adg-1-127.pdf). Adv Geosci 1:127–135

Schrama E (1986) Estimability of potential coefficients from orbit perturbations. In: Reports of the Departmant of Geodesy, Mathematical and Physical Geodesy 86.1. Delft University of Technology

Schrama E (1995) Gravity research missions reviewed in light of the indirect ocean tide potential. In: Rapp RH, Nerem RS (eds) In: Proceedings IUGG symposium, Boulder

Schuh WD (1996) Tailored numerical solution strategies for the global determination of the Earth's gravity field. Mitteilungen der geodätischen Institute der Technischen Universität Graz. Folge 81. Graz

Sneeuw NJ, Gerlach C, Švehla D, Gruber C (2002) A first attempt at time-variable gravity recovery from CHAMP using the energy balance approach (available as http://olimpia.topo.auth.gr/GG2002/SESSION3/Sneeuw.pdf). In: Proceedings of the 3rd meeting of the international gravity and geoid commission. Thessaloniki, Greece, 26–30 August

Standish EM (1998) JPL Planetary and Lunar Ephemerides, DE405/LE405. JPL IOM 312.F-98-048

Teunissen PJG (2000) Testing theory: an introduction. Delft University Press, Delft

Tikhonov AN, Arsenin VY (1977) Solutions of ill-posed problems. V.H. Winston and Sons, Washington

van den IJssel J, Visser P, Rodriguez EP (2003) CHAMP precise orbit determination using GPS data. Adv Space Res 31:1889–1895

Švehla D, Rothacher M (2003) Kinematic precise orbit determination for gravity field determination (available as http://tau.fesg.tu-muenchen.de/ drazen/IUGG03_Svehla.pdf). In: Proceedings of the IUGG General Assembly, Sapporo, Japan, 30 June – 11 July, 2003